FLOW PAST BLUFF BODIES

Thad S. Morton

Department of Mechanical Engineering, Brigham Young University, Provo, UT 84602

Abstract

More than a century ago Kirchhoff solved for the velocity distribution within an elliptical patch of uniform vorticity. That solution became the basis for all further studies of elliptical vortices and has been regarded as the only known exact solution for a steady, elliptical patch of uniform vorticity. In the present paper, an exact solution for a new elliptical patch of uniform vorticity is presented. The vortex is constructed of streamlines of constant eccentricity. By specifying a velocity distribution along either of the principle axes of the vortex, continuity between differentially-spaced streamlines provides the velocity distribution throughout the vortex. Some of the unique features of the vortex are that although the vorticity is uniform throughout the vortex, the angular velocity about the center is non-uniform, unlike the Kirchhoff vortex wherein both are uniform. The point of maximum velocity occurs not at the end of the major axes as in the case of Kirchhoff's vortex, but rather at the end of the minor axes, more nearly approximating the behavior of the twin vortices formed behind bluff bodies. In the present work, a non-orthogonal (non-confocal) elliptical coordinate system is employed to solve for the velocity and pressure distributions within the vortex.

Introduction

The study of flow past bluff bodies is broad, involving a variety of challenging problems, ranging from flame stabilization by means of bluff-body flameholders in ramjet and turbojet afterburners (Stwalley *et al.* 1988), to the well-known problem of galloping conductors (Zdero *et al.* 1995) and stall flutter associated with wings, propellers and compressor and turbine blades (Bisplinghoff *et al.* 1955) caused by vortex-induced oscillations. The principle of vortex shedding from a bluff body is also a well known method of flow measurement (Turner *et al.* 1993). Much current research focuses on designing wings so as to trap a vortex above an airfoil section in an effort to produce high lift during landing and takeoff (see for example, Slomski and Coleman 1993 and Rossow 1992). Under certain conditions wake flows may experience cavitation at points of minimum pressure within the flow. In a review of cavitation inception, Rood (1991), noted that a major hindrance to understanding the interaction between expanding nuclei and the underlying flow structure is the lack of knowledge about the dynamics of the flow structures in the single-phase flow.

Bluff-body flow problems still rely almost entirely upon experimental or numerical data for their solution. This requires that proposed body shapes be handled case by case, if any quantitative information is to be known. Presently, the upper limit on direct numerical simulation of such flows is on the order of $Re \approx 1000$. Numerical solutions of all other flows typically employ turbulence models. The major difficulty in theoretically predicting flow properties, heat transfer rates, etc. for bluff-body flows lies in the separated boundary layer. The capability of predicting flow property distributions along the front surface of a body is crucially dependent on conditions in the near wake region of the body. This flow region is characterized by highly vortical flow. The main problems encountered when trying to apply conventional boundary layer theory to separated boundary layers is the uncertainty as to the location of and pressure at the point of separation. Cavity and wake models have grown increasingly elaborate. In all past theoretical models for separated flow, the pressure within the wake bubble, and hence along the separated streamline, is assumed to be constant. Moreover, in each of the practical flow models "an artifice of some sort is introduced," as remarked by Wu (1968), to allow the cavitation number to be a free parameter in order to account for viscous dissipation in the wake. This allows potential theory to then be applied to the resulting flow. Otherwise, a potential flow analysis of a finite wake bubble yields the dilemma of zero drag on the body. Wu (1968) also pointed out that a removal of flow energy directly from the potential flow in order to simulate viscous dissipation would require a removal of momentum, or mass, or both. It is this dilemma which the flow models attempt to overcome. The standard assumption of constant pressure within the wake is considered to be supported by experimental measurements of conditions immediately behind the body (Fage and Johansen 1927), which show that the pressure is "nearly constant." However, as noted by Thwaites (1960, p. 106), Fage and Johansen also found that the pressure coefficient close behind the flat plate

(referred to as the *base pressure coefficient*) was about $c_{p_b} = -1.4$, while at infinity $c_p = 0$. He then made the following remark:

> "This suggests the more plausible assumption that the pressure varies along the bounding streamline... But although mathematical methods are available to solve the external inviscid flow once this pressure distribution is known, they do not indicate how it is to be determined at the start. This is the greatest immediate difficulty in the theory of well-separated flows: if it could be overcome it is likely that the concept of the free streamline would survive for a long time to give way only to a detailed theory of the flow within the wake and its interaction with the inviscid region."

For supersonic flows, the hyperbolic nature of the outer flow simplifies the establishment of the inviscid flow configuration as well as a base pressure; however, for incompressible flows, the elliptic nature of the equations makes it necessary to find the outer flow and the wake geometry simultaneously. As remarked by Chow (1976), "It is apparent that this type of flow offers the most complicated and challenging problems." While theoretical models of such flows are many, there remains to be found a single analytical solution describing the pressure distribution within a bluff-body wake. From flow visualizations of the stationary, twin vortices formed in the near wake of bluff bodies (Prandtl and Tietjens 1934; Taneda 1956; Taneda 1968; Van Dyke 1982), it appears that bluff-body wake vortices preserve the axis ratio of concentric elliptical streamlines. These ellipses are not confocal. The first analytical solution for this type of elliptical vortex was obtained as part of the present research.

Wakeless Flow

The original objective of the present work was to understand how the heat transfer along the front of a curved surface varies with surface curvature in separated flows. As a preliminary investigation, the solution for unseparated flow past a curved surface was obtained by a series of conformal transformations. The resulting dimensionless velocity profile along the curved surface is shown in Fig. 1 as a function of surface curvature. The curvature parameter, h, is the maximum distance between the surface and the chord; therefore, a value of $h = 0$ corresponds to a flat plate and $h = 1$ to a semi-circular cylinder.

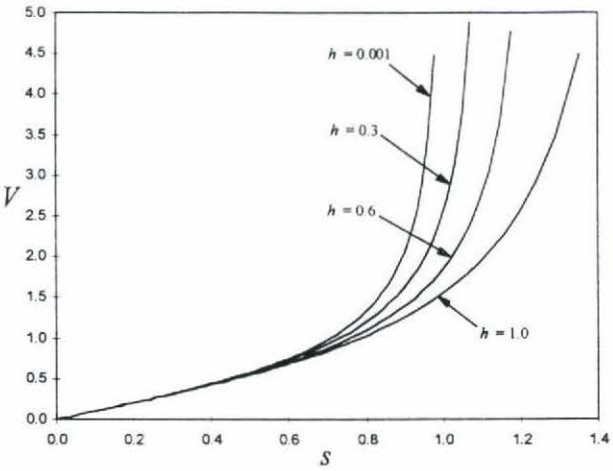

Fig. 1. Variation in dimensionless velocity profile with plate curvature.

As seen from the figure, curvature of the plate appears to have little effect on the velocity distribution in the neighborhood of the stagnation point. The dimensionless length, s, is the arc length normalized by the projected plate width (twice the x-coordinate of the surface endpoint in this case); therefore, for large values of curvature, the dimensionless flow path, s, is seen to be larger than unity.

Wake Flow

As indicated in last year's report, free streamline theory is inadequate to treat separated flow past surfaces with curvature. In this classical approach to separated flows, the outer flow is uncoupled from the wake by some assumption about the base pressure coefficient. This assumption must be empirically-based, if an accurate representation of the velocity profile along the front surface is hoped for. The common thread which appears in separated flows past any bluff body shape is the pair of stationary vortices which form in the wake. At large Reynolds numbers, the effect of body shape (including surface curvature) on the time-mean wake structure seems to be an almost second-order effect. It was, therefore, thought that useful information could be gained by studying the vortices formed within a wake. At low Reynolds numbers ($Re < 45$ for a cylinder, for example), a pair of standing vortices form and elongate into ellipses with increasing Reynolds number. More than a century ago Kirchhoff (1876) solved for the velocity distribution within an elliptical patch of uniform vorticity (see also Lamb 1932). However, this elliptical vortex, observed visually, appears unsuited for the description of typical wake vortices.

The Coordinate System

The general approach will be to find an elliptical coordinate system wherein contours of one of the contravariant components, $\bar{x}^1$ say, of the position vector of a fluid particle coincides with the vortex streamlines, as observed from flow visualizations cited in the Introduction. From these visualizations, the eccentricity of the twin vortices in the near wake region appears to be constant. Secondly, the mass flow rates passing through both principle axes (as well as any other axis through the origin) must be equal. But in order for this integration to be performed with respect to a single coordinate, it is convenient to make contours of the other coordinate pass through the origin. One such coordinate system is:

$$x^1 = \bar{x}^1 A\cos\left(\bar{x}^2\right)$$

$$x^2 = \bar{x}^1 B\sin\left(\bar{x}^2\right)$$

$$x^3 = \bar{x}^3$$

where x^k are the coordinates of a typical fluid particle relative to a rectangular coordinate system. For studying the twin vortices behind bluff bodies, this coordinate system has two major advantages over the orthogonal coordinate system of confocal ellipses. First, the eccentricity of the ellipse is constant even for a change in the first coordinate. Second, integration for the mass flow rate can be performed along lines of constant $\bar{x}^2$ because they all pass through the origin. Defining the constants A and B as follows

$$A = \cosh(q), \qquad B = \sinh(q), \qquad q > 0$$

allows the axis ratio of concentric ellipses to remain constant as $\bar{x}^1$ and $\bar{x}^2$ vary independently. It also ensures the useful identity:

$$A^2 - B^2 = 1. \tag{1}$$

The coordinate system is shown in Fig. 2. The metric tensor for this coordinate system is:

$$\bar{g}_{ij} = \sum_k \frac{\partial x^k}{\partial \bar{x}^i}\frac{\partial x^k}{\partial \bar{x}^j}$$

$$\bar{g}_{ij} = \begin{bmatrix} \cos^2\left(\bar{x}^2\right) + B^2 & -\bar{x}^1\sin\left(\bar{x}^2\right)\cos\left(\bar{x}^2\right) & 0 \\ -\bar{x}^1\sin\left(\bar{x}^2\right)\cos\left(\bar{x}^2\right) & \left(\bar{x}^1\right)^2\left[A^2 - \cos^2\left(\bar{x}^2\right)\right] & 0 \\ 0 & 0 & 1 \end{bmatrix}$$

As seen from the off-diagonal elements, the coordinate system is orthogonal only when $\bar{x}^2 = 0, \pi/2, \pi, 3\pi/4, \ldots$ The Jacobian determinant is $\sqrt{\bar{g}} = \bar{x}^1 AB$.

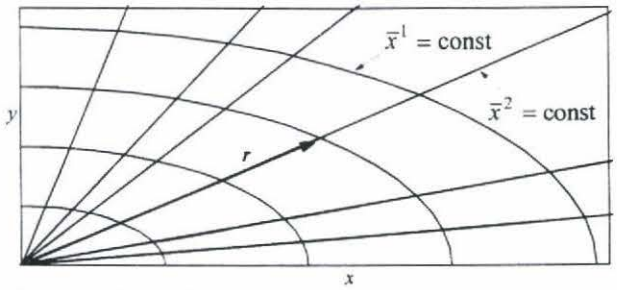

Fig. 2. Non-orthogonal, elliptic coordinate system.

Solution Method

A Geometrical Relationship

The angle, θ, of a cylindrical system is related to the "angle," $\bar{x}^2$, of the non-confocal, elliptical coordinate system by:

$$\tan\theta = \frac{x^2}{x^1} = \frac{\bar{x}^1 B\sin\left(\bar{x}^2\right)}{\bar{x}^1 A\cos\left(\bar{x}^2\right)} = \frac{B}{A}\tan\left(\bar{x}^2\right)$$

Note that the two angles are equal only at points where the elliptic coordinate system is orthogonal. Taking the derivative with respect to time of $\tan\theta$ to get a relation for the fluid angular velocity about the origin and using the fact that $r\cos\theta = \bar{x}^1 A\cos\left(\bar{x}^2\right)$, yields

$$\bar{v}^2 = \frac{d\bar{x}^2}{dt} = \frac{1}{AB}\left(\frac{r}{\bar{x}^1}\right)^2\frac{d\theta}{dt} \tag{2}$$

The ratio $\left(\frac{r}{\bar{x}^1}\right)$ can be found from the definition of the coordinate system to vary as follows:

$$\frac{r}{\bar{x}^1} = \sqrt{A^2\cos^2\left(\bar{x}^2\right) + B^2\sin^2\left(\bar{x}^2\right)}. \tag{3}$$

Velocity Vector Components

A relationship between the velocity vector components, $\bar{v}^k = \frac{d\bar{x}^k}{dt}$, and the magnitude, $|\mathbf{v}|$ from the following inner product:

$$|\mathbf{v}|^2 = (\mathbf{v}\cdot\mathbf{v}) = \bar{v}_k\bar{v}^k.$$

Raising the index of the covariant component allows the velocity magnitude to be expressed in terms of the

square of the contravariant velocity components in the barred system, as follows:

$$|\mathbf{v}|^2 = \bar{g}_{jk}\bar{v}^j\bar{v}^k$$

Here the only nonzero velocity component is $\bar{v}^2$ (recall that the curves $\bar{x}^1 = \text{const.}$ are streamlines across which no fluid passes). With this simplification,

$$\bar{v}^2 = \frac{|\mathbf{v}|}{\sqrt{\bar{g}_{22}}} \tag{4}$$

Conservation of Mass

The mass flow rate passing between the origin and any point on the perimeter of the vortex is expressed as follows:

$$\dot{m} = \int_A \rho(\mathbf{v}\cdot\mathbf{n})dA \tag{5}$$

Where $\mathbf{n}$ is the unit normal to the area dA. The limits of this integral vary depending upon the angle at which the integration is performed. However, if the integration is performed in terms of the elliptical coordinates, the second coordinate, $\bar{x}^2$, will remain constant throughout the integration (see Fig. 2), and the limit, c, for the integral over $\bar{x}^1$ will also remain constant ($c = b/B$) regardless of the path chosen for integration. To implement this transformation the Jacobian enters into the integrand, as follows:

$$\dot{m} = -\int_{\bar{x}^1=0}^{c}\int_{\bar{x}^3=0}^{L}\rho\bar{v}^2\sqrt{\bar{g}}\,d\bar{x}^3 d\bar{x}^1$$

$$\dot{m} = -L\int_{\bar{x}^1=0}^{c}\rho\bar{v}^2\left(\bar{x}^1 AB\right)d\bar{x}^1$$

The equivalent differential flow rate equation is:

$$\delta\dot{m} = -L\rho AB\bar{x}^1\bar{v}^2 d\bar{x}^1, \tag{6}$$

which gives the mass flow rate between differentially-spaced streamlines. For a constant-density fluid, it must have the same value when evaluated at any value of $\bar{x}^2$ so long as $\bar{x}^1$ remains constant, that is

$$\delta\dot{m}(\bar{x}^1, \pi/2) = \delta\dot{m}(\bar{x}^1, \bar{x}^2) \qquad \forall\ \bar{x}^2.$$

Substituting Eq. (6) into this expression of mass conservation gives a relation for the velocity component in the elliptical coordinate system:

$$\left(L\rho AB\bar{x}^1\bar{v}^2 d\bar{x}^1\right)\Big|_{(\bar{x}^1,\,\pi/2)} = \left(L\rho AB\bar{x}^1\bar{v}^2 d\bar{x}^1\right)\Big|_{(\bar{x}^1,\,\bar{x}^2)}$$

$$\bar{v}^2\Big|_{(\bar{x}^1,\,\pi/2)} = \bar{v}^2\Big|_{(\bar{x}^1,\,\bar{x}^2)}$$

Since the angle, $\bar{x}^2$, was arbitrary, $\bar{v}^2$ is the same for all $\bar{x}^2$, so long as $\bar{x}^1$ remains constant. The quantity on the left will be replaced by Eq. (4), and the quantity on the right by Eq. (2). With these substitutions, the rotation rate about the origin becomes

$$\frac{d\theta}{dt} = \frac{B|\mathbf{v}|\Big|_{(\bar{x}^1,\,\pi/2)}}{\bar{x}^1\left(A^2\cos^2\bar{x}^2 + B^2\sin^2\bar{x}^2\right)}. \tag{7}$$

Equation (7) gives the angular velocity of any particle of fluid about the origin. However, some assumption must be made as to the velocity magnitude along the semi-minor axis.

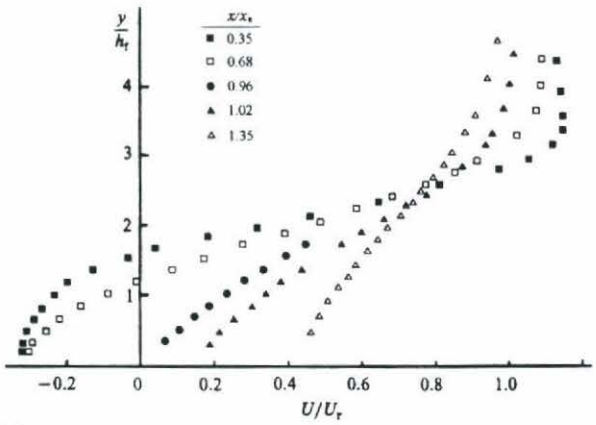

(a)

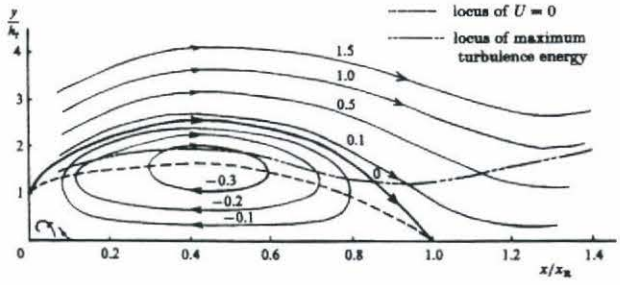

(b)

Fig. 3. Wake behind a normal flat plate with long trailing splitter plate. $Re = 23{,}000$. (a) Mean velocity profiles, (b) Mean streamlines. x_R is the mean reattachment length. (Castro and Haque 1987).

Experimental measurements of this velocity, made by Castro and Haque (1987), are shown in Fig. 3. These measurements, as well as those of Armstrong and

Barnes (1987) and Yang and Tsai (1992), show a linear variation in velocity with vertical distance from the vortex center to the perimeter. If this velocity magnitude is chosen to be a linear function of distance from the origin, that is if

$$|\mathbf{v}|_{(\bar{x}^1,\pi/2)} = \Omega_d r\Big|_{(\bar{x}^1,\pi/2)} = \Omega_d \bar{x}^1 B, \qquad (8)$$

where the proportionality constant Ω_d is the instantaneous angular velocity along the semi-minor axis, then the angular velocity of the vortex given by (7), denoted now by $\Omega(\bar{x}^2)$, is

$$\Omega(\bar{x}^2) = \frac{B^2\Omega_d}{A^2\cos^2\bar{x}^2 + B^2\sin^2\bar{x}^2}. \qquad (9)$$

Notice that the angular velocity is not uniform throughout the domain.

Substituting Eq. (9) into (2) we find that

$$\bar{v}^2 = \frac{B}{A}\Omega_d, \qquad (10)$$

which is a constant value. Then by Eq. (4), the fluid velocity magnitude is

$$|\mathbf{v}| = \frac{B}{A}\Omega_b \bar{x}^1\sqrt{A^2 - \cos^2(\bar{x}^2)} \qquad (11)$$

Notice that at any given angle, $\bar{x}^2$, the velocity *magnitude* is a linear function of $\bar{x}^1$, the constant of proportionality depending upon the value of $\bar{x}^2$.

The velocity distribution may be transformed to the rectangular coordinate system by means of the transformation

$$v^i = \frac{\partial x^i}{\partial \bar{x}^j}\bar{v}^j.$$

The velocity distribution then becomes:

$$\mathbf{v} = \begin{bmatrix} -y \\ x\left(\frac{b}{a}\right)^2 \\ 0 \end{bmatrix}\Omega_d \qquad (12)$$

Notice that the maximum velocity occurs along the broad side of the ellipse.

Calculating the Vorticity Distribution

Denoting the permutation symbol by ε^{ijk} and the permutation tensor by E^{ijk}, the vorticity may be expressed in the rectangular system as:

$$\omega = (\nabla \times \mathbf{v})$$

$$\omega^i = \varepsilon^{ijk}v_{k,j} = E^{ijk}v_{k,j}$$

The permutation symbol and tensor coincide in the rectangular system. Expressing the relation in terms of the permutation tensor provides a proper tensor relation valid in any coordinate system; therefore, in the barred system:

$$\bar{\omega}^i = \bar{E}^{ijk}\bar{v}_{k,j} = \frac{\varepsilon^{ijk}}{\sqrt{\bar{g}}}\bar{v}_{k,j}.$$

Following the rules for covariant differentiation of a covariant tensor of order one, the velocity gradient expands as follows:

$$\bar{\omega}^i = \frac{\varepsilon^{ijk}}{\sqrt{\bar{g}}}\left[\frac{\partial \bar{v}_k}{\partial \bar{x}^j} - \bar{\Gamma}^m_{kj}\bar{v}_m\right] \qquad (13)$$

where $\bar{\Gamma}^m_{kj}$ is the Christoffel symbol of the second kind given by

$$\bar{\Gamma}^m_{kj} = \frac{1}{2}\bar{g}^{mp}\left(\frac{\partial \bar{g}_{pk}}{\partial \bar{x}^j} + \frac{\partial \bar{g}_{pj}}{\partial \bar{x}^k} - \frac{\partial \bar{g}_{kj}}{\partial \bar{x}^p}\right).$$

By direct computation, it can be shown that the only non-zero Christoffel symbols correspond to those of a cylindrical coordinate system, namely:

$$\bar{\Gamma}^2_{12} = \bar{\Gamma}^2_{21} = \frac{1}{\bar{x}^1} \quad \text{and} \quad \bar{\Gamma}^1_{22} = -\bar{x}^1. \qquad (14)$$

When $i = 3$, Eq. (13) becomes:

$$\bar{\omega}^3 = \frac{\varepsilon^{312}}{\sqrt{\bar{g}}}\left[\left(\frac{\partial \bar{v}_2}{\partial \bar{x}^1} - \bar{\Gamma}^p_{21}\bar{v}_p\right) - \left(\frac{\partial \bar{v}_1}{\partial \bar{x}^2} - \bar{\Gamma}^p_{12}\bar{v}_p\right)\right]$$

The velocities are known in terms of the contravariant components rather than the covariant components. Raising the index of the covariant velocity components and canceling the two symmetric Christoffel symbols, $\bar{\Gamma}^p_{12}$ and $\bar{\Gamma}^p_{21}$, gives:

$$\bar{\omega}^3 = \frac{1}{\sqrt{\bar{g}}}\left[\frac{\partial}{\partial \bar{x}^1}\left(\bar{g}_{p2}\bar{v}^p\right) - \frac{\partial}{\partial \bar{x}^2}\left(\bar{g}_{p1}\bar{v}^p\right)\right]$$

The only non-zero component of velocity in the barred system is obtained when $p = 2$. Substitution of Eq. (4)

for the velocity magnitude into the above equation then yields:

$$\overline{\omega}^3 = \frac{1}{\sqrt{\overline{g}}}\left[\frac{\partial}{\partial \overline{x}^1}\left(\sqrt{\overline{g}_{22}}|\mathbf{v}|\right) - \frac{\partial}{\partial \overline{x}^2}\left(\frac{\overline{g}_{21}|\mathbf{v}|}{\sqrt{\overline{g}_{22}}}\right)\right]$$

The vorticity can be further simplified by substituting Eq. (11), differentiating, and employing (1) to obtain:

$$\overline{\omega}^3 = \Omega_d\left(1+\frac{b^2}{a^2}\right). \tag{15}$$

Similar reasoning yields the identities $\overline{\omega}^1 = \overline{\omega}^2 = 0$. Therefore, the vorticity of the flow is uniform and drops by half in the limit of large axis ratio. This constitutes a new solution for an elliptical patch of uniform vorticity.

Verifying the Solution

It can be verified by direct substitution that the solution satisfies the steady equations of continuity and momentum for an incompressible, Newtonian fluid:

$$(\nabla \cdot \mathbf{v}) = 0 \tag{16}$$

$$\mathbf{v}\cdot\nabla\boldsymbol{\omega} = \boldsymbol{\omega}\cdot\nabla\mathbf{v} + \nu\nabla^2\boldsymbol{\omega} \tag{17}$$

The second of the above equations, called the vorticity equation, was obtained by taking the curl of the momentum equation.

Calculating the Pressure Distribution

Having verified that the velocity distribution is in fact a solution to the system given by Eqs. (16) and (17), the momentum equation

$$\frac{1}{2}\rho\nabla(\mathbf{v}\cdot\mathbf{v}) - \rho(\mathbf{v}\times\boldsymbol{\omega}) = -\nabla p + \mu\nabla^2\mathbf{v} \tag{18}$$

can now be used to find the pressure distribution within the vortex. The last term is seen to be zero by inspection of the velocity distribution (12) which is linear in the two independent variables. The Laplacian in rectangular coordinates immediately yields the zero vector. Therefore, the motion is such that the shear stress is zero throughout the vortex. In other words, the inner vortex driven by a shear layer will eventually behave as an inviscid fluid as $t \to \infty$.

Written in covariant tensor form, Eq. (18) is:

$$\frac{1}{2}\rho\left(\overline{v}_k\overline{v}^k\right)_{,i} - \rho\overline{E}_{ijk}\overline{v}^j\overline{\omega}^k = -\overline{p}_{,i}$$

The first term of the equation contains a covariant velocity; however, the velocity is known in terms of the contravariant components. Making this change of variance and the substitution for the permutation tensor gives:

$$\frac{1}{2}\rho\left(\overline{g}_{kp}\overline{v}^p\overline{v}^k\right)_{,i} - \rho\sqrt{\overline{g}}\,\varepsilon_{ijk}\overline{v}^j\overline{\omega}^k = -\overline{p}_{,i} \tag{19}$$

Applying Ricci's theorem (see Borisenko and Tarapov 1968) allows the metric tensor to be brought out of the covariant differentiation. The first term of Eq. (19) then becomes:

$$\frac{1}{2}\rho\overline{g}_{kp}\left(\overline{v}^p\overline{v}^k\right)_{,i} = \frac{1}{2}\rho\overline{g}_{kp}\left[\frac{\partial\left(\overline{v}^p\overline{v}^k\right)}{\partial\overline{x}^i} + \overline{\Gamma}^p_{mi}\overline{v}^m\overline{v}^k + \overline{\Gamma}^k_{ni}\overline{v}^p\overline{v}^n\right]$$

By inspection of the indices on the velocity components, the only values of m and n which survive the summation are $m = n = 2$. The partial derivatives also vanish. This gives:

$$\frac{1}{2}\rho\overline{g}_{kp}\left(\overline{v}^p\overline{v}^k\right)_{,i} = \frac{1}{2}\rho\overline{g}_{kp}\left[\overline{\Gamma}^p_{2i}\overline{v}^2\overline{v}^k + \overline{\Gamma}^k_{2i}\overline{v}^p\overline{v}^2\right]$$

Summing on p and k and eliminating all zero-valued velocity components, gives:

$$\frac{1}{2}\rho\overline{g}_{kp}\left(\overline{v}^p\overline{v}^k\right)_{,i} = \rho\left(\overline{v}^2\right)^2\left[\overline{g}_{12}\overline{\Gamma}^1_{2i} + \overline{g}_{22}\overline{\Gamma}^2_{2i}\right]$$

So for $i = 1$, we have:

$$\frac{1}{2}\rho\overline{g}_{kp}\left(\overline{v}^p\overline{v}^k\right)_{,1} = \rho\left(\overline{v}^2\right)^2\bar{x}^1\left(A^2 - \cos^2\bar{x}^2\right) \tag{20}$$

and for $i = 2$,

$$\frac{1}{2}\rho\overline{g}_{kp}\left(\overline{v}^p\overline{v}^k\right)_{,2} = \rho\left(\overline{v}^2\right)^2\left(\bar{x}^1\right)^2\sin\left(\bar{x}^2\right)\cos\left(\bar{x}^2\right) \tag{21}$$

which is the same result that would be obtained if instead the velocity *magnitude* were simply differentiated following the rules for covariant differentiation of a scalar invariant.

The second term in Eq. (19) is expanded below:

$$-\rho\sqrt{\overline{g}}\,\varepsilon_{ijk}\overline{v}^j\overline{\omega}^k = -\rho\sqrt{\overline{g}}\,\varepsilon_{i23}\overline{v}^2\overline{\omega}^3$$

By inspection, the only indices which survived the summation are $j = 2$ and $k = 3$. By definition of the permutation symbol, the only non-zero component appears when $i = 1$. Therefore, the only non-zero component of the second term in Eq. (19) is:

$$-\rho\sqrt{\bar{g}}\varepsilon_{123}\bar{v}^j\bar{\omega}^k = -\rho\bar{x}^1 B^2\Omega_d{}^2\left(1+\left(\frac{b}{a}\right)^2\right) \qquad (22)$$

Each of the terms in the momentum equation is now known with the exception of the pressure gradient. Solving Eq. (18) for the pressure gradient gives

$$\nabla p = -\frac{1}{2}\rho\nabla(\mathbf{v}\cdot\mathbf{v}) + \rho(\mathbf{v}\times\boldsymbol{\omega})$$

Expanding each of the terms on the right in the barred coordinate system using Eqs. (20) through (22), we have

$$\begin{bmatrix}\bar{p}_{,1}\\ \bar{p}_{,2}\\ \bar{p}_{,3}\end{bmatrix} = \rho\left(\frac{b}{a}\right)^2\Omega_d{}^2\bar{x}^1\begin{bmatrix}\cos^2(\bar{x}^2)+B^2\\ -\bar{x}^1\sin(\bar{x}^2)\cos(\bar{x}^2)\\ 0\end{bmatrix}$$

As in the case of a circular vortex, a trade off occurred in the radial component of the pressure gradient between the first and second terms. The positive contribution to the pressure gradient made by the vorticity term dominates, so that the pressure decreases toward the center. Integrating the second component of the pressure gradient with respect to $\bar{x}^2$ gives:

$$\bar{p} = \int\frac{\partial\bar{p}}{\partial\bar{x}^2}d\bar{x}^2 = \frac{\rho}{2}\left(\frac{b}{a}\right)^2\Omega_d{}^2\left(\bar{x}^1\right)^2\cos^2(\bar{x}^2)+f(\bar{x}^1)$$

Integrating the first component of the pressure gradient with respect to $\bar{x}^1$, we have:

$$\bar{p}' = \int\frac{\partial\bar{p}}{\partial\bar{x}^1}d\bar{x}^1$$

$$\bar{p}' = \frac{\rho}{2}\left(\frac{b}{a}\right)^2\Omega_d{}^2\left(\cos^2(\bar{x}^2)+B^2\right)\left(\bar{x}^1\right)^2+h(\bar{x}^2)$$

In order to find the functions $f(\bar{x}^1)$ and $h(\bar{x}^2)$ we can require that $\bar{p}-\bar{p}'=0$, so that the pressure distribution within the vortex becomes:

$$\bar{p} = \frac{\rho}{2}\left(\frac{b}{a}\right)^2\Omega_d{}^2\left(\bar{x}^1\right)^2\left(A^2\cos^2(\bar{x}^2)+B^2\sin^2(\bar{x}^2)\right)+c_1$$

where the identity (1) has been used. Since the pressure is a scalar invariant, its transformation is trivial: $p=\bar{p}$. Using the definition of the coordinate system, the pressure can then be expressed in rectangular coordinates as

$$p-p_c = \frac{1}{2}\rho\left(\Omega_d r\right)^2\left(\frac{b}{a}\right)^2 \qquad (23)$$

Setting the center pressure, p_c, equal to the vapor pressure of the fluid gives the condition for incipient cavitation in the case of a liquid. It is interesting that contours of pressure remain circular even as the vortex elongates. Increased vortex eccentricity only reduces the radial pressure gradient, effectively causing the spacing between pressure contours to increase. The pressure distribution given by Eq. (23) increases quite slowly with r compared with that of the Kirchhoff vortex. In fact, for equal axis ratios and equal *driving velocities*, (defined as $v_b=\Omega_b b$, the velocity at the point $(0,b)$), the pressure within the Kirchhoff vortex increases at a rate which is at least 3 times that of the present vortex. This characteristic of the present vortex is favorable since the pressure distribution in the wake bubble behind a bluff body is not far from uniform (Fage and Johansen 1927). Furthermore, the relationship between the present elliptical vortex and its circular pressure contours is supported by numerical visualizations made by Fornberg (1985) of the circular cylinder wake and also by Tamura *et al.* (1993) in a study of rectangular cylinders. A comparison is shown in Fig. 4 of the pressure variation through a vortex center for the two vortices. The figures show that the pressure is more uniform in the present vortex. If the outer pressures of the two vortices are considered equal, it is apparent that the pressure does not drop as low towards the center of the present vortex as it does in the Kirchhoff vortex. Note also from Fig. 4(b) that increased vortex eccentricity increases the difference in center and outer pressures in the Kirchhoff vortex but decreases it in the present vortex.

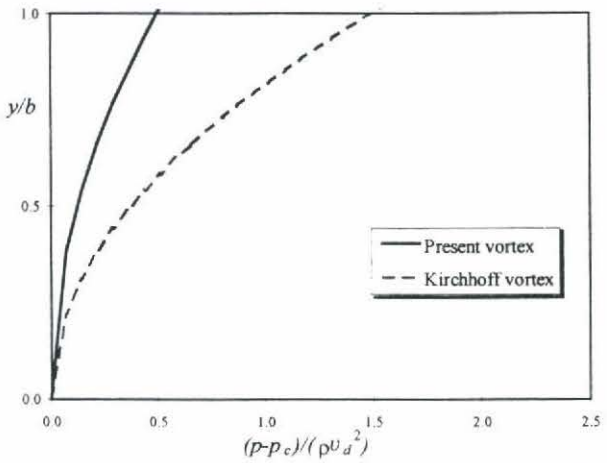

Fig. 4. (a) Comparison of Kirchhoff vortex and the present vortex vertical centerline pressure variation for axis ratio of $a/b=1$.

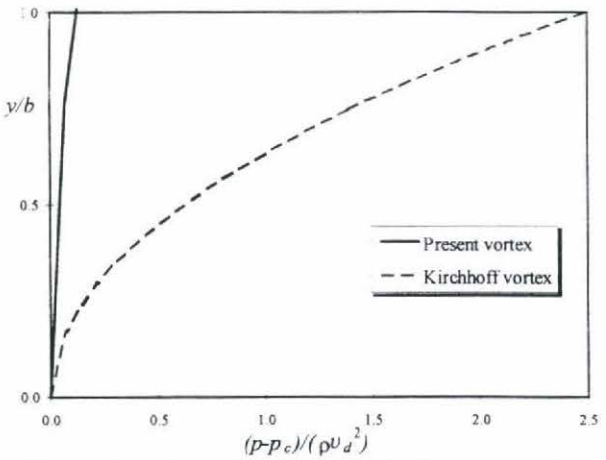

Fig. 4. (b) Comparison of Kirchhoff vortex and the present vortex vertical centerline pressure variation for axis ratio of $a/b = 2$.

Shape Characterization through Vortex Eigenvalues

The system (12) of ordinary differential equations may be put into the form:

$$\dot{\mathbf{x}} = \mathbf{A}\,\mathbf{x} \tag{24}$$

where the transformation matrix in two dimensions is given by:

$$\mathbf{A} = \begin{bmatrix} 0 & -\Omega_d \\ \left(\frac{b}{a}\right)^2 \Omega_d & 0 \end{bmatrix}$$

The solution to (24) is $\mathbf{x}(t) = e^{\mathbf{A}t}\mathbf{x}_0$, where $\mathbf{x}_0$ is the initial position of a fluid particle at time $t = 0$. The eigenvalues of this system are $\lambda_1 = i\frac{b}{a}\Omega_d$ and $\lambda_2 = -i\frac{b}{a}\Omega_d$, which correspond to a stable center in phase space, as expected. Here it is evident that the physical vortex is being represented as a non-dissipative dynamical system. This could also have been deduced by the vanishing of the viscous stress term in Eq. (18). In reality, the stationary vortex is sustained because energy dissipation is offset by kinetic energy input along the broad side of the vortex by the free stream (see Batchelor 1956).

The system matrix **A** can be reduced to Jordan canonical form and exponentiated to obtain the position of any fluid particle in the vortex expressed as a function of time and its initial position:

$$x(t) = x_0 \cos\left(\frac{b}{a}\Omega_d t\right) - \frac{a}{b} y_0 \sin\left(\frac{b}{a}\Omega_d t\right)$$

$$y(t) = x_0 \frac{b}{a} \sin\left(\frac{b}{a}\Omega_d t\right) + y_0 \cos\left(\frac{b}{a}\Omega_d t\right)$$

It is noteworthy that the eigenvalues for the Kirchhoff vortex are $\lambda_{K1} = i\Omega_b$ and $\lambda_{K2} = -i\Omega_b$. A distinguishing feature of the eigenvalues of the present vortex then is that the rotation rate along the minor axis is normalized by the degree to which the vortex is elongated. Consider the eigenvalues of the present vortex in the following form:

$$\lambda_{1,2} = \pm i\frac{U_d}{a}.$$

In the flow regime characterized by the standing eddies (roughly $Re \le 40$ for cylinders), the length of the wake bubble, which is proportional to a, apparently varies linearly with Reynolds number, regardless of the obstacle shape (Taneda 1956; Grove *et al.* 1964; Acrivos *et al.* 1968; Taneda 1968; Dennis and Chang 1970; Fornberg 1985). From experimental measurements in the wake of various bluff bodies at high Reynolds numbers ($100 \le \mathrm{Re} \le 10^5$), the driving velocity, U_d, will likely remain on the same order of magnitude as the free stream velocity, the ratio of the two being nearly unity. This suggests that the vortex eigenvalue remains constant as the flow speed, and hence the length of the wake bubble, increases. If the vortex eigenvalue is independent of the flow speed in this initial Reynolds number range, what then is it a function of? By comparison of the wakes of various body shapes, such as normal flat plates and circular cylinders (see Prandtl and Tietjens 1934; Van Dyke 1982), the eigenvalue appears to characterize the obstacle shape.

Conclusion

The solution of a new elliptical patch of uniform vorticity has been presented which more closely resembles the standing vortices found in bluff-body wakes than the conventional vortex. It was then showed that in standing eddy flow, obstacles may be characterizable by the eigenvalues of the vortices formed in their wakes. While the Kirchhoff vortex has been studied extensively in the past, the vortex introduced in the present paper has remained virtually unstudied. Therefore, issues such as its relation to shear flow, its stability, its behavior in unsteady flow, etc. have never been investigated. Future plans include an application to drag prediction and a numerical simulation of low Reynolds number flow past a normal flat plate.

Acknowledgments

The research was supported in part by the Rocky Mountain NASA Space Grant Consortium, EL 302, Logan, UT 84322-4140.

Literature Cited

Acrivos, A., Leal, L. G., Snowden, D. D., and Pan, F., 1968, "Further experiments on steady separated flows past bluff objects," *J. Fluid Mech.*, Vol. 34, pp. 25-48.

Armstrong, B. J., and Barnes, F. H., 1987, "A comparison of the structure of the wake behind a circular cylinder in a steady flow with that in a perturbed flow," *Phys. Fluids*, Vol. 30, pp. 19-26.

Batchelor, G. K., 1956, "On steady laminar flow with closed streamlines at large Reynolds number," *J. Fluid Mech.*, Vol. 1, pp. 177-190.

Bisplinghoff, R. L., Ashley, H., and Halfman, R. L., 1955, *Aeroelasticity* Addison-Wesley (Dover, NY, 1996).

Borisenko, A. I., and Tarapov, I. E., 1968, *Vector and Tensor Analysis with Applications*, Dover, New York.

Castro, I. P., and Haque, A., 1987, "The structure of a turbulent shear layer bounding a separation region," *J. Fluid Mech.*, Vol. 179, pp. 439-468.

Chow, W. L., and Spring, D. J., 1976, "Viscid-Inviscid Interaction of Incompressible Separated Flows," *Journal of Applied Mechanics*, Vol. 43, pp. 387-395.

Dennis, S. C. R., and Chang, G.-Z., 1970, "Numerical solutions for steady flow past a circular cylinder at Reynolds numbers up to 100," *J. Fluid Mech.*, Vol. 42, pp. 471-489.

Fage, A and Johansen, F. C., 1927, "On the Flow of Air behind an Inclined Flat Plate of Infinite Span," *Proceedings of the Royal Society of London* A, Vol. 116, pp. 170-197.

Fage, A and Johansen, F. C., 1928, "The structure of the vortex street," *Phil. Mag.*, Vol. 5, pp. 417-441.

Fornberg, B., 1985, "Steady Viscous Flow Past a Circular Cylinder up to Reynolds Number 600," *Journal of Computational Physics*, Vol. 61, p. 297-320.

Grove, A. S., Shair, F. H., Petersen, E. E., and Acrivos, A., 1964, "An experimental investigation of the steady separated flow past a circular cylinder," *J. Fluid Mech.*, Vol. 19, pp. 60-81.

Kirchhoff, G., 1876, *Vorlesungen über Matematische Physik*, Vol. 1, Leipzig: Teubner, 466 pp.

Lamb, H., 1932, *Hydrodynamics*, Dover, NY; (Cambridge University Press, NY, 1993).

Prandtl, L., and Tietjens, O. G., 1934, *Applied Hydro- and Aeromechanics*, Dover, NY.

Rood, E., 1991, "Review - Mechanisms of Cavitation Inception," *ASME Journal of Fluids Engineering*, Vol. 113, pp. 163-175.

Rossow, V. J., 1992, "Two-fence concept for efficient trapping of vortices on airfoils," *Journal of Aircraft*, Vol. 29, No. 5, pp. 847-855.

Slomski, J. F., and Coleman, R. M., 1993, "Numerical simulation of vortex generation and capture above an airfoil," *31st Aerospace Sciences Meeting and Exhibit, January 11-14, 1993, Reno, Nevada, AIAA Paper* 93-864, 11 pp.

Stwalley, R. M. III, and Lefebvre, A. H., 1988, "Flame Stabilization Using Large Flameholders of Irregular Shape," *J. Propulsion*, Vol. 4, pp. 4-13.

Tamura, T., Itoh, Y., and Kuwahara, K., 1993, "Computational separated-reattaching flows around a rectangular cylinder," *Journal of Wind Engineering and Industrial Aerodynamics*, Vol. 50, pp. 9-18.

Taneda, S., 1956, "Experimental investigations of the wakes behind cylinders and plates at low Reynolds numbers," *J. Phys. Soc. Japan*, Vol. 11, pp. 302-307.

Taneda, S., 1968, "Standing twin-vortices behind a thin flat plate normal to the flow," *Reports of Research Institute for Applied Mechanics*, Vol. 16, pp. 155-163.

Thwaites, B., 1960, *Incompressible Aerodynamics*, Clarendon, Oxford.

Turner, J. T., Popiel, C. O., and Robinson, D. I., 1993, "Evolution of an improved vortex generator," *Flow Meas. Instrum.*, Vol. 4, No. 4, pp. 249-258.

Van Dyke, M., 1982, *An Album of Fluid Motion*, The Parabolic Press, Stanford, CA.

Wu, T. Y., 1968, "Inviscid cavity and wake flows," in *Basic Developments in Fluid Dynamics*, Vol. 2, pp. 1-116.

Yang, J.-T., and Tsai, G.-L., 1992, "The Wake Flow Structure of an Open-Slit V Gutter," *Experimental Thermal and Fluid Science*, Vol. 5, pp. 685-696.

Zdero, R., Turan, Ö. F., and Havard, D. G., 1995, "Toward Understanding Galloping: Near-Wake Study of Oscillating Smooth and Stranded Circular Cylinders in Forced Motion," *Experimental Thermal and Fluid Science*, Vol. 10, pp. 28-43.